CHINESE OPTICS LETTERS

Vol. 20, No. 11 | November 2022

High-fidelity parametric amplification of Ince–Gaussian beams

Ding Yan (闫 顶), Zhiyuan Zhong (钟致远), Tong Qi (齐 桐), Hongying Chen (陈洪影), and Wei Gao (高 玮)*

Heilongjiang Provincial Key Laboratory of Quantum Control, School of Measurement and Communication Engineering, Harbin University of Science and Technology, Harbin 150080, China

*Corresponding author: wei_g@163.com

Received March 16, 2022 | Accepted June 10, 2022 | Posted Online July 14, 2022

Ince–Gaussian (IG) beams, as eigenfunctions of the paraxial wave equation in elliptical coordinates, are attracting increasing interest owing to their propagation-invariant and full-field properties. Optical amplification via parametric interactions can further expand their application areas, yet it is rarely studied. In this work, we report on a high-fidelity parametric amplifier for IG beams. The nonlinear transformation of the spatial spectra of the signal and associated influences on the beam profiles of the amplified signal, under different pump structures, were theoretically and experimentally investigated. By using a perfect flattop beam as the pump, we show that the transverse structure of IG signals is well maintained, and the distortion induced by radial-mode degeneration is overcome during amplification. This proof-of-principle demonstration paves the way for a mode-independent and distortion-free amplifier of arbitrary structured light and has great significance in relevant areas, such as quantum optics, tunable infrared-laser generation, and image amplification.

Keywords: optical parametric amplification; Ince–Gaussian beam; high fidelity; perfect flattop beam.
DOI: 10.3788/COL202220.113801

1. Introduction

Soon after Franken *et al.* observed second-harmonic generation[1], Kingston *et al.* proposed an optical parametric oscillator in 1962[2,3], and then Wang and Racetle first, to the best of our knowledge, observed parametric gain of the laser in $NH_4H_2PO_4$ (ADP) crystals in 1965[4]. Subsequent research and further development of optical parametric amplification (OPA) have received significant attention due to its ability to amplify weak signals with high and ultra-broadband gain, meanwhile, generating the difference frequency light (i.e., idler beam). This technique has been applied in various areas such as strong-field physics, tunable infrared-laser generation, and noiseless image amplification[5–9]. The emergence of structured light represented by beams carrying orbital angular momentum (OAM) renewed broad research interest[10–14]. Beyond the OAM, structured light, in principle, can be extended to all degrees of freedom and dimensions, which has revived many areas ranging from classical to quantum light and fundamental physics to advanced photonic techniques[15–19]. Structured light can typically be generated by low-peak-power devices such as liquid-crystal spatial light modulators (SLMs)[20], digital micromirror devices[21–23], q-plates[24], and other spin-orbit approaches[25–27]. The need for structured light demonstrations at higher powers for industrial applications has remained an open challenge[10]. OPA is an alternative method to obtain high-power structured light. The OPA of OAM-carrying beams and the transformation of OAM were studied both theoretically and experimentally[28–30]. Polarization-insensitive OPA of radially polarized femtosecond pulses was also successfully achieved with high gain[31].

More recently, the nonlinear interaction of the full-field modes with the azimuthal and radial structure has attracted much interest. The nonlinear transformation of full-field Laguerre–Gaussian (LG) modes was realized in the OPA and parametric up-conversion[30,32]. Ince–Gaussian (IG) beams have a natural full-field transverse structure with well-defined Gouy phases and can be regarded as superpositions of LG modes. Moreover, IG beams exhibit propagation-invariant or diffraction-free properties, and helical IG modes carry OAM, which makes them applicable in optical communication, quantum key distribution, and particle manipulation. In some applications, the amplification of IG beams is required for long-distance propagation and nonlinear interaction. However, there have been few reports on this topic; in the current stage, it is still a challenge for high-fidelity amplification of IG beams and nonlinear transformation during amplification.

In this work, we report the high-fidelity parametric amplification of IG beams for the first time, to the best of our knowledge. Through theoretical simulations and experimental verification, we show that IG beams can be amplified without

changing their transverse structure by using a perfect flattop beam as the pump. In contrast, the transverse structure of the beam was changed when a common Gaussian beam was used as the pump. Furthermore, we measured output signal energy and gain factor for different IG modes under the flattop pump condition and confirmed mode-independent OPA in principle.

2. Theoretical Analysis

IG beams are exact solutions of the paraxial wave equation in the elliptical cylindrical coordinates. Such beams can be classified according to their parity into even and odd modes, which can be expressed as[33]

$$\begin{aligned} \mathrm{IG}^{e}_{n,m}(r,z;\varepsilon) &= \frac{Cw_0}{w(z)} C^m_n(i\xi,\varepsilon) C^m_n(\eta,\varepsilon) e^{-\frac{r^2}{w^2(z)}} e^{-i\Phi(r,z)}, \\ \mathrm{IG}^{o}_{n,m}(r,z;\varepsilon) &= \frac{Sw_0}{w(z)} S^m_n(i\xi,\varepsilon) S^m_n(\eta,\varepsilon) e^{-\frac{r^2}{w^2(z)}} e^{-i\Phi(r,z)}, \end{aligned} \tag{1}$$

where the superscripts e and o refer to the even modes and odd modes, respectively; $C^m_n(\cdot)$ $[S^m_n(\cdot)]$ denotes even (odd) Ince polynomials of order n and degree m, and C (S) is the associated normalization constant. The indices (n,m) satisfy the conditions $0 \le m \le n$ for even functions and $1 \le m \le n$ for odd functions; $w(z)$ is the beam radius as a function of the propagation distance z, and $w(z=0) = w_0$ denotes the Gaussian beam waist; $\Phi(r,z)$ can be given by $kz + kr^2/2R(z) - (n+1)\arctan(z/z_R)$, with $R(z)$ the curvature radius of the wavefront, z_R the Rayleigh length, and $(n+1)\arctan(z/z_R)$ the Gouy phase accumulated during the diffraction propagation. Furthermore, the ellipticity parameter ε is a characteristic factor in the ellipse coordinate system. The transitions from IG modes to LG and Hermite–Gaussian (HG) modes occur as the elliptic coordinates tend to the circular cylindrical and Cartesian coordinates, i.e., $\varepsilon \to 0$ and $\varepsilon \to \infty$, respectively.

IG beams can also be represented as a conjugate superposition of $(n+1)$ LG modes. For $\varepsilon > 0$, $\mathrm{IG}^{e(o)}_{n,m}$ can be given by[33]

$$\mathrm{IG}^{e(o)}_{n,m} = \sum_p a_p \mathrm{LG}^{\pm\ell}_p, \qquad p \in \{0, 1, \ldots, (n-1)/2\}, \tag{2}$$

where the complex coefficient a_p denotes modal weights, i.e., spatial spectra or wave functions in the momentum space. ℓ (p) is the azimuthal (radial) index of the LG modes, and every LG mode has the same order $n = 2p + |\ell|$. This implies that the IG modes have the full-field and propagation-invariant transverse profiles.

The basic requirement for an ideal spatial-mode laser amplifier should ensure that the transverse structure of the signal is maintained, and the gain is independent of the signal modes. Here, we used a single-pass OPA platform for demonstrating high-fidelity and mode-independent amplification of IG modes. An IG signal beam (ω_1) and a pump beam (ω_3) interact in the nonlinear crystal to generate the amplified signal (ω_1) and idler beam $(\omega_2 = \omega_3 - \omega_1)$, and phase matching requires a dispersion relation $k_3(\omega_3) = k_1(\omega_1) + k_2(\omega_2)$. For simplicity, we assume that the OPA is operated in the small-signal amplification regime (i.e., pump nondepletion), and, when the phase matching is satisfied, the slowly varying complex amplitudes of the interacting waves are coupled by[34]

$$\frac{\mathrm{d}A_s}{\mathrm{d}z} = \frac{2i\omega_1^2 d_{\mathrm{eff}}}{k_1 c^2} A_p(0) A_i^*(z), \tag{3}$$

$$\frac{\mathrm{d}A_i}{\mathrm{d}z} = \frac{2i\omega_2^2 d_{\mathrm{eff}}}{k_2 c^2} A_p(0) A_s^*(z), \tag{4}$$

where $A_p(0)$ is the pump wave amplitude at the input of the crystal, $A_{s(i)}$ denotes the signal (idler) wave amplitude, and d_{eff} is the effective value of the nonlinear susceptibility tensor. The solution to Eqs. (3) and (4) that meets the boundary of $A_i(0) = 0$ is given by[34]

$$A_s(z) = A_s(0)\cosh \kappa z, \tag{5}$$

$$A_i(z) = i\left(\frac{n_1\omega_2}{n_2\omega_1}\right)^{1/2} \frac{A_p}{|A_p|} A_s^*(0)\sinh \kappa z, \tag{6}$$

where κ is the real coupling constant given by

$$\kappa = \frac{2d_{\mathrm{eff}}\omega_1\omega_2}{c^2\sqrt{k_1 k_2}} A_p(0). \tag{7}$$

Equations (5)–(7) can be used to calculate the transverse profiles of the amplified signal and the idler wave.

Without loss of generality, $\mathrm{IG}^{e}_{4,0}$ and $\mathrm{IG}^{o}_{4,2}$ in elliptical coordinates with $\varepsilon = 2$ are chosen as the signals. They can be represented as superposition states of the LG modes of order $n = 2p + |\ell| = 4$, i.e., LG spectra of the signals, according to Eq. (2), which can be expressed as

$$\begin{aligned} \mathrm{IG}^{e}_{4,0} &= 0.115\mathrm{LG}^{\pm4}_0 + 0.617\mathrm{LG}^{\pm2}_1 + 1.10\mathrm{LG}^{0}_2, \\ \mathrm{IG}^{o}_{4,2} &= 0.290\mathrm{LG}^{\pm4}_0 + 0.957\mathrm{LG}^{\pm2}_1. \end{aligned} \tag{8}$$

It can be seen from Eq. (8) that the IG beams are the full-field spatial modes in polar coordinates and are non-separable with respect to the azimuthal and radial indices. We first consider the OPA pumped by a more commonly used Gaussian (TEM_{00}) beam. Figures 1(a) and 1(b) show the LG spectra of $\mathrm{IG}^{e}_{4,0}$ and $\mathrm{IG}^{o}_{4,2}$ signals and their amplification with different pump beam sizes, respectively. Here, the waist radius of pump beams (w_p) is chosen as one, two, and three times the signal waist (w_s). Compared with the input IG signals, we can see that more radial components appear in the LG spectra of amplified signals. Moreover, the weight of these components decreases with the w_p of the pump beam and gradually closes into those of the original signals when $w_p > 3w_s$. In addition, the signal gain factor also has an impact on the radial-mode composition of the signal, as shown in Fig. 1(c), where the radial components increase with the gain. These indicate that considerable radial-mode

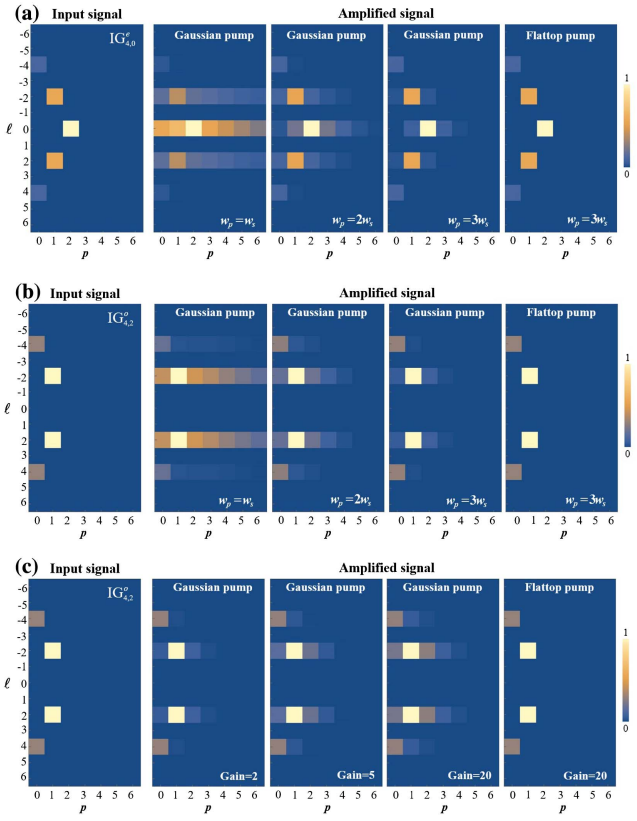

Fig. 1. LG spectra of input signal and amplified signal pumped by Gaussian and flattop beams. (a) and (b) show the cases of $w_p = w_s$, $2w_s$, and $3w_s$ for $IG^e_{4,0}$ and $IG^o_{4,2}$ signals at gain of 2, respectively. (c) LG spectra with different gain factors at $w_p = 3w_s$.

degeneration, i.e., generating new radial modes (e.g., $LG_2^{\pm 2}$, $LG_0^{\pm 2}$, LG_3^0, LG_1^0), is introduced into $LG_1^{\pm 2}$ and LG_2^0 during the OPA under the Gaussian pump condition. Thus, the order of these new radial modes, i.e., $2p + |\ell|$, is not unified, breaking the synchronization of the Gouy phase, which induces an evolution of the intensity distribution during propagation. Consequently, their beam profile would no longer be propagation invariant. In other words, the OPA pumped by the rotationally symmetric Gaussian beam is more sensitive to radial components than to the azimuthal ones, leading to the distortion of spatial modes. Only using the pump beam with a large enough size can alleviate the distortion induced by the radial-mode degeneration; at this time, the pump has an approximately uniform interaction with the input signals. As seen in Fig. 1, the LG spectra are well maintained when using a flattop beam as the pump and $w_p = 3w_s$, even for the case of high gain. Therefore, the flattop beam that is independent of the radial mode is an alternative option as the pump.

3. Simulation and Experiment Results

Figure 2 shows a diagram of the experimental setup, where a pulsed Nd:$Y_3Al_5O_{12}$ (Nd:YAG) laser with 10 ns pulse duration

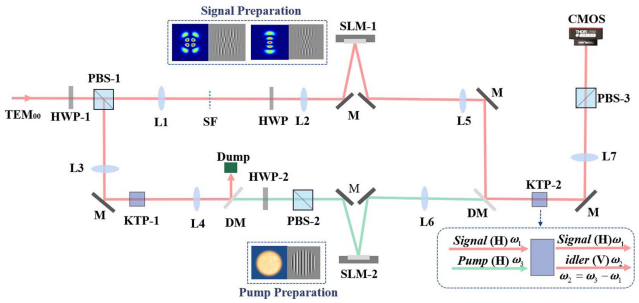

Fig. 2. Diagram of the OPA experimental setup, where the key components include the mirror (M), lenses (L1-L7), polarizing beam splitter (PBS), half-wave plate (HWP), spatial light modulator (SLM), spatial filter (SF), beam profiler (CMOS), and dichroic mirror (DM).

and 1 Hz repetition frequency, set at 1064 nm wavelength, was used as the source for preparing pump and signal beams. Using a half-wave plate (HWP-1) in combination with a polarizing beam splitter (PBS-1) separated the beam into transmitted and reflected parts. The transmitted part was converted into the target IG modes with the modulation from SLM-1 (Hamamatsu X13138-09 1272X1024 pixels, 12.5 μm pixel size) for use as the signals. For preparing the pump, the reflected part was focused into a 6 mm long $KTiOPO_4$ (KTP-1) crystal (1064 nm → 532 nm) to obtain a 532 nm beam. A combination of HWP-2 and PBS-2 was utilized to adjust the pump power and form the horizontally (H) polarized light. Then, it was sent to SLM-2 (Holoeye PLUTO VIS-096, 1920X1080 pixels, 8 μm pixel size) to convert the pump into either flattop or Gaussian beams with variable beam sizes. The prepared pump and signal beams with H polarization were combined using a dichroic mirror (DM) and then focused into a 6 mm long KTP-2 crystal (type-II OPA, its schematic illustration is shown on the right bottom of Fig. 2). PBS-3 was used to separate the signal (H) and the idler with vertical polarization (V) before the camera, and the amplified signal was characterized by a CMOS-based beam profiler.

We considered only small signals in undepleted regimes to focus on the influence of spatial modes on the nonlinear interaction. In the experiment, the pump and signal had the energy of ~1.0 mJ and ~50 nJ, respectively. Taking $IG^e_{4,0}$ mode as an example, Figs. 3(b) and 3(c) show the simulated and observed beam profiles of the amplified signals at the position of $z = 0$ and $z \to \infty$ when using the Gaussian pump with one and two times the signal waist. It should be noted that far-field intensity profiles are different from the near-field ones, i.e., the spatial-mode distortions occur and are propagation variant due to the presence of the radial-mode degeneration. The theoretical analysis mentioned above was well confirmed by the experimental results.

To overcome the distortion induced by the radial-mode degeneration, we used a perfect flattop beam as a pump, whose complex amplitude can be expressed as $E_p^{\omega_3}(z) = A_p(0) \cdot \exp[-ik(\omega_3)z]$. The term 'perfect flattop' means that its amplitude and phase are both spatially uniform and efficiently cover

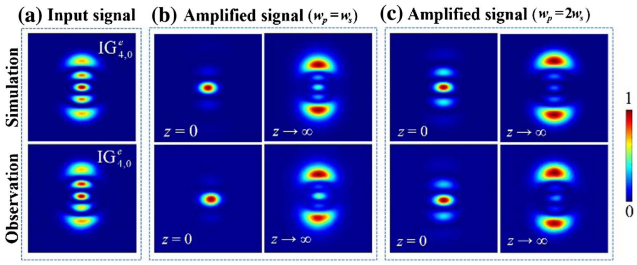

Fig. 3. Simulated and experimentally observed results of the OPA pumped by a Gaussian beam, where (a) shows the IG signal profiles; (b) and (c) are corresponding amplified signal profiles with $w_p = w_s, 2w_s$, respectively.

IG signals at the focal region within the crystal. According to Eqs. (5)–(7), the spatial structure of signals is not affected by the pump during the OPA. Notably, the commonly used flattop beam obtained via computer-generated holography based on phase-only modulation can only provide a flattop intensity distribution but not include the phase[35,36], which will disturb the phase profile and hence the propagation property of the signal in the nonlinear interaction. Here, the perfect flattop beam was designed based on the super-Gaussian mode, i.e., $u_{SG}(r, \varphi) = \exp[-(r/w)^n]$, with an order $n = 12$ and prepared via computer-generated holography based on complex-amplitude modulation, as shown by the grating pattern near SLM-2 in Fig. 2. This flattop beam is useful, particularly for structured light with complex phase profiles. Detailed descriptions of its generation are out of the scope of this paper and will be addressed in another publication.

Figures 4(b) and 4(c) show the beam profiles of the prepared signals and their corresponding amplification in the far field, respectively. They agree well with each other as well as with their theoretical references, shown in Fig. 4(a). It can be seen that the transverse structure of two types of IG modes is efficiently maintained in the OPA. In the experiment and simulation, the waist ratio of the pump and signal beams is chosen as ~3:1; at this time, the flattop area of the pump can totally cover the IG signals, as shown in the inset of Fig. 5. To quantitatively show this excellent agreement, we compare the far-field amplified light

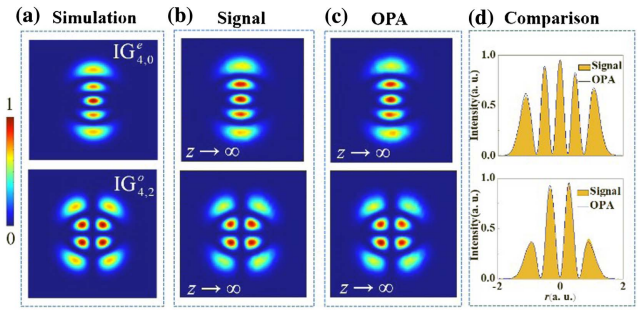

Fig. 4. Results of the OPA pumped by a flattop beam, where (a)–(c) show the theoretical beam profiles, the measured signals, and the corresponding amplified signals, respectively; (d) comparison of the far-field amplified light and the input signal obtained via experimental observation.

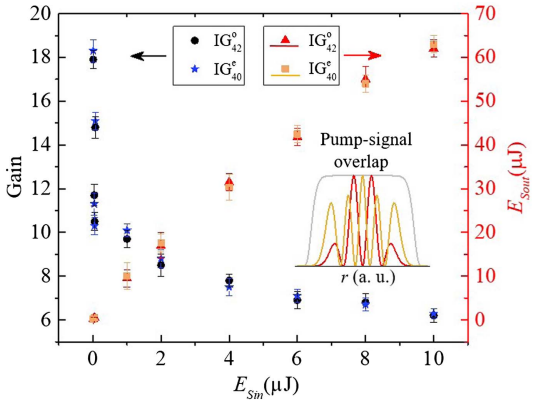

Fig. 5. Measured amplified signal energy and gain factor versus the input signal energy for IG-mode OPA. Inset, the overlap of the pump, $IG^e_{4,0}$, and $IG^o_{4,2}$ signals.

and the input signal, obtained via experimental observation, as depicted in Fig. 4(d). The inner products of the matrix between corresponding intensity profiles are > 0.98, which shows high fidelity in the flattop pump OPA process. Furthermore, amplified signals inherit the propagation-invariant property of IG beams, indicating that the identity of the Gouy phase is also well preserved. These are attributed to the fact that the perfect flattop pump did not disturb the spatial-mode complex amplitude during the interactions.

We finally studied the amplified signal gain and output energy (E_{sout}) as a function of input signal energy (E_{sin}) for the flattop pump, as shown in Fig. 5.

The pump beam has constant energy of ~1.3 mJ. We can see from Fig. 5 that in the experiment the signal gain of ~18 was achieved for the signal energy of below ~50 nJ, and the maximum amplified signal energy was ~63 μJ when the signal energy was set at ~10 μJ. Notably, the signal gains are almost the same over the error range for $IG^e_{4,0}$ and $IG^o_{4,2}$ modes. This indicates that the amplification gain is independent of the signal modes under the flattop pump, where the pump was optimized to adequately cover these modes within the crystal, as shown in the inset of Fig. 5. Moreover, the gain or efficiency can be enhanced by increasing the power of the pump or optimizing crystal parameters. Therefore, the flattop pump can not only adequately maintain the spatial-mode spectrum of the signal to overcome the distortion, but also achieve the mode-independent amplification gain.

4. Conclusion

In summary, we theoretically and experimentally studied the parametric amplifier of IG beams. We showed that for full-field modes involving azimuthal and radial compositions, such as IG beams, the commonly used Gaussian pump gave rise to spatial-mode distortion of amplified output beams. The distortion was caused by new radial-mode generation during the OPA. By using the perfect flattop beam as the pump, we realized the

IG-mode OPA without changing the transverse structure and the amplification gain independent of the input signal. This proof-of-principle work enables high-fidelity amplification for arbitrary structured light and provides a wider range of applications in classical and quantum optics for the generalized higher-order modes.

Acknowledgement

This work was supported by the National Natural Science Foundation of China (NSFC) (Nos. 62075050 and 61975047) and the High-Level Talents Project of Heilongjiang Province (No. 2020GSP12).

References

1. P. A. Franken, A. E. Hill, C. W. Peters, and G. Weinreich, "Generation of optical harmonics," Phys. Rev. Lett. **7**, 118 (1961).
2. R. H. Kingston, "Parametric amplification and oscillation at optical frequencies," Proc. IRE **50**, 472 (1962).
3. N. M. Kroll, "Parametric amplification in spatially extended media and application to the design of tuneable oscillators at optical frequencies," Phys. Rev. **127**, 1207 (1962).
4. C. C. Wang and G. W. Racette, "Measurement of parametric gain accompanying optical difference frequency generation," Appl. Phys. Lett. **6**, 169 (1965).
5. J. Ma, J. Wang, P. Yuan, G. Xie, K. Xiong, Y. Tu, X. Tu, E. Shi, Y. Zheng, and L. Qian, "Quasi-parametric amplification of chirped pulses based on a Sm^{3+}-doped yttrium calcium oxyborate crystal," Optica **2**, 1006 (2015).
6. H. Suchowski, G. Porat, and A. Arie, "Adiabatic processes in frequency conversion," Laser Photonics Rev. **8**, 333 (2014).
7. A. Mosset, F. Devaux, and E. Lantz, "Spatially noiseless optical amplification of images," Phys. Rev. Lett. **94**, 223603 (2005).
8. F. Devaux and E. Lantz, "Gain in phase sensitive parametric image amplification," Phys. Rev. Lett. **85**, 2308 (2000).
9. C. Dorrer, "Optical parametric amplification of spectrally incoherent pulses," J. Opt. Soc. Am. B **38**, 792 (2021).
10. A. Forbes, M. de Oliveira, and M. R. Dennis, "Structured light," Nat. Photon. **15**, 253 (2021).
11. M. J. Padgett, "Orbital angular momentum 25 years on [Invited]," Opt. Express **25**, 11265 (2017).
12. Y. Shen, X. Wang, Z. Xie, C. Min, X. Fu, Q. Liu, M. Gong, and X. Yuan, "Optical vortices 30 years on: OAM manipulation from topological charge to multiple singularities," Light Sci. Appl. **8**, 90 (2019).
13. A. E. Willner, H. Huang, Y. Yan, Y. Ren, N. Ahmed, G. Xie, C. Bao, L. Li, Y. Cao, Z. Zhao, J. Wang, M. P. J. Lavery, M. Tur, S. Ramachandran, A. F. Molisch, N. Ashrafi, and S. Ashrafi, "Optical communications using orbital angular momentum beams," Adv. Opt. Photon. **7**, 66 (2015).
14. J. Chen, C. Wan, and Q. Zhan, "Engineering photonic angular momentum with structured light: a review," Adv. Photon. **3**, 064001 (2021).
15. R. F. Offer, A. Daffurn, E. Riis, P. F. Griffin, A. S. Arnold, and S. Franke-Arnold, "Gouy phase-matched angular and radial mode conversion in four-wave mixing," Phys. Rev. A **103**, L021502 (2021).
16. G. Vallone, V. D'Ambrosio, A. Sponselli, S. Slussarenko, L. Marrucci, F. Sciarrino, and P. Villoresi, "Free-space quantum key distribution by rotation-invariant twisted photons," Phys. Rev. Lett. **113**, 060503 (2014).
17. Z. Zhu, M. Janasik, A. Fyffe, D. Hay, Y. Zhou, B. Kantor, T. Winder, R. W. Boyd, G. Leuchs, and Z. Shi, "Compensation-free high-dimensional free-space optical communication using turbulence-resilient vector beams," Nat. Commun. **12**, 1666 (2021).
18. A. G. de Oliveira, M. F. Z. Arruda, W. C. Soares, S. P. Walborn, R. M. Gomes, R. Medeiros de Araújo, and P. H. Souto Ribeiro, "Real-time phase conjugation of vector vortex beams," ACS Photonics **7**, 249 (2020).
19. R. Zhong, Z. Zhu, H. Wu, C. Rosales-Guzmán, S. Song, and B. Shi, "Gouy-phase-mediated propagation variations and revivals of transverse structure in vectorially structured light," Phys. Rev. A **103**, 053520 (2021).
20. G. Lazarev, P. Chen, J. Strauss, N. Fontaine, and A. Forbes, "Beyond the display: phase-only liquid crystal on silicon devices and their applications in photonics [Invited]," Opt. Express **27**, 16206 (2019).
21. Y. Ren, R. Lu, and L. Gong, "Tailoring light with a digital micromirror device," Ann. Phys. **527**, 447 (2015).
22. C. Rosales-Guzmán, X. Hu, A. Selyem, P. Moreno-Acosta, S. Franke-Arnold, R. Ramos-Garcia, and A. Forbes, "Polarisation-insensitive generation of complex vector modes from a digital micromirror device," Sci. Rep. **10**, 10434 (2020).
23. S. Turtaev, I. T. Leite, K. J. Mitchell, M. J. Padgett, D. B. Phillips, and T. Čižmár, "Comparison of nematic liquid-crystal and DMD based spatial light modulation in complex photonics," Opt. Express **25**, 29874 (2017).
24. A. Rubano, F. Cardano, B. Piccirillo, and L. Marrucci, "Q-plate technology: a progress review [Invited]," J. Opt. Soc. Am. B **36**, D70 (2019).
25. F. Cardano and L. Marrucci, "Spin–orbit photonics," Nat. Photon. **9**, 776 (2015).
26. K. Y. Bliokh, F. J. Rodríguez-Fortuño, F. Nori, and A. V. Zayats, "Spin–orbit interactions of light," Nat. Photon. **9**, 796 (2015).
27. L. Marrucci, E. Karimi, S. Slussarenko, B. Piccirillo, E. Santamato, E. Nagali, and F. Sciarrino, "Spin-to-orbital conversion of the angular momentum of light and its classical and quantum applications," J. Opt. **13**, 064001 (2011).
28. A. G. de Oliveira, G. Santos, N. R. da Silva, L. J. Pereira, G. B. Alves, A. Z. Khoury, and P. H. S. Ribeiro, "Beyond conservation of orbital angular momentum in stimulated parametric down-conversion," Phys. Rev. Appl. **16**, 044019 (2021).
29. R. B. Rodrigues, G. B. Alves, R. F. Barros, C. E. R. Souza, and A. Z. Khoury, "Generalized orbital angular momentum symmetry in parametric amplification," Phys. Rev. A **105**, 013510 (2022).
30. X. Fang, H. Yang, Y. Zhang, and M. Xiao, "Optical parametric amplification of a Laguerre–Gaussian mode," OSA Continuum **2**, 236 (2019).
31. H. Zhong, C. Liang, S. Dai, J. Huang, S. Hu, C. Xu, and L. Qian, "Polarization-insensitive, high-gain parametric amplification of radially polarized femtosecond pulses," Optica **8**, 62 (2021).
32. H. Wu, L. Mao, Y. Yang, C. Rosales-Guzmán, W. Gao, B. Shi, and Z. Zhu, "Radial modal transitions of Laguerre-Gauss modes during parametric up-conversion: towards the full-field selection rule of spatial modes," Phys. Rev. A **101**, 063805 (2020).
33. M. A. Bandres and J. C. Gutierrez-Vega, "Ince-Gaussian beams," Opt. Lett. **29**, 144 (2004).
34. R. W. Boyd, *Nonlinear Optics* (Elsevier, 2010).
35. D. Nodop, J. Ruecker, S. Waechter, and M. Kahle, "Hyperbolic phase function used in a spatial light modulator for flat top focus generation," Opt. Lett. **44**, 2169 (2019).
36. A. Kobyakov, M. Sauer, and D. Chowdhury, "Stimulated Brillouin scattering in optical fibers," Adv. Opt. Photon. **2**, 1 (2010).